

Fastened Aluminum-Lipped Channel Sections Subjected to Web Crippling under Two-Flange Loading Conditions: Experimental Study

Author

Alsanat, Husam, Gunalan, Shanmuganathan, Keerthan, Poologanathan, Guan, Hong, Baniotopoulos, Charalampos

Published

2020

Journal Title

Journal of Structural Engineering

Version

Accepted Manuscript (AM)

DOI

[10.1061/\(ASCE\)ST.1943-541X.0002550](https://doi.org/10.1061/(ASCE)ST.1943-541X.0002550)

Rights statement

© 2019 American Society of Civil Engineers (ASCE). This is the author-manuscript version of this paper. Reproduced in accordance with the copyright policy of the publisher. Please refer to the journal's website for access to the definitive, published version.

Downloaded from

<http://hdl.handle.net/10072/399982>

Griffith Research Online

<https://research-repository.griffith.edu.au>

Fastened Aluminium Lipped Channel Sections Subjected to Web Crippling under Two-Flange Loading Conditions - Experimental Study

Husam Alsanat^{1a,b}, Shanmuganathan Gunalan², Poologanathan Keerthan³, Hong Guan⁴ and
Charalampos Baniotopoulos⁵

^{1a} Ph.D Researcher, School of Engineering and Built Environment, Griffith University, Gold
Coast, Australia. Email: husam.alsanat@griffithuni.edu.au

^{1b} Sponsored Ph.D student, School of Engineering, Al-Hussein Bin Talal University, Ma'an,
Jordan. Email: hosam.r.alsannat@ahu.edu.jo

² Senior Lecturer, School of Engineering and Built Environment, Griffith University, Nathan,
Australia. E-mails: s.gunalan@griffith.edu.au

³ Associate Professor, Faculty of Engineering and Environment, University of Northumbria,
Newcastle, UK. E-mails: keerthan.poologanathan@northumbria.ac.uk

⁴ Professor, School of Engineering and Built Environment, Griffith University, Gold Coast,
Australia. Email: h.guan@griffith.edu.au

⁵ Professor, Department of Civil Engineering, University of Birmingham, Birmingham, UK.
E-mails: c.baniotopoulos@bham.ac.uk

ABSTRACT

Thin-walled members in structural systems are highly vulnerable to buckling instabilities including web crippling. Aluminium alloy members are more prone to this kind of failure due to their relatively low elastic moduli. As shown in the existing literature, limited research has been performed to investigate the web crippling failure of aluminium members. Therefore, this paper presents the details of an experimental investigation conducted to study the web crippling phenomenon of fastened (restrained flanges) aluminium lipped channel (ALC) sections. Two loading conditions of End-Two-Flange (ETF) and Interior-Two-Flange

26 (ITF) were considered. Two series of 40 tests were performed using roll-formed aluminium
27 alloy 5052 H36 specimens with different web slenderness and load bearing lengths. A
28 comparison between the ultimate capacities of the web crippling tests and the predictions from
29 the currently available design rules was performed. The results show that the current web
30 crippling design rules are mostly unsafe and unreliable for fastened ALC sections. Thus, a
31 modified equation is needed to closely and accurately estimate the web crippling strengths for
32 fastened ALC sections under two-flange loading conditions. Furthermore, the influence of
33 restrained flanges on the web crippling mechanism was discussed in detail. It was observed
34 that fastening the flanges considerably strengthened the section web crippling capacity; hence
35 a new prediction approach was developed to estimate the increase of the web crippling capacity
36 due to flange restraining.

37 **Keywords:** Web crippling; Aluminium lipped channel sections; Experimental study; Fastened;
38 Two-flange loading conditions, Design rules.

39 INTRODUCTION

40 Aluminium alloy sections fabricated using roll-forming technique are becoming
41 increasingly popular in structural applications including roofing and flooring systems, modular
42 structures and various types of structures in corrosive environments. Figure 1 shows an
43 application of roll-formed ALC section as purlins in Minto reservoir roof – NSW, Australia.
44 Thin-walled flexural members may be loaded by inducing a concentrated load at either the load
45 application point between supports or by way of the reactions at the supports. This could
46 potentially lead to a localized web crippling failure. The AISI S909 (2008) Standard test
47 method for determining the web crippling strength of cold-formed steel beams considers two
48 loading conditions that thin-walled members may be subjected to in a structural system. End-

49 loading condition refers to when the distance between the end of the member and edge of the
50 bearing plate is equal or less than to 1.5 times the flat portion of the web (h); otherwise, it is
51 classified as interior-loading condition. Each load conditions are also classified into two groups
52 according to the application of the transverse compression load on one-flange or two-flanges.
53 The one-flange loading condition is considered if the distance between the edges of two
54 opposite bearing plates is more than $1.5h$. Otherwise, it is considered as a two-flange loading
55 condition. These prime loading conditions are classified as: end-one-flange (EOF), interior-
56 one-flange (IOF), end-two-flange (ETF), and interior-two-flange (ITF) loading conditions. In
57 addition, these cases can be further classified according to the flange connections, fastened and
58 unfastened. Figures 2 (a) and (b) show the cases included in this study, fastened ETF and ITF
59 loading conditions, while Figure 2 (c) presents the geometrical profile of a lipped channel
60 section.

61 Extensive experimental research has been carried out to investigate the web crippling
62 mechanism of thin-walled members. The majority of the previous studies were performed on
63 cold-formed steel sections in which the sections were not attached (unfastened) to the supports
64 (Sundararajah et al. ((2016), (2017)), Gunalan and Mahendran ((2015), (2019)), Keerthan et al
65 (2014), Keerthan and Mahendran (2016) and Steau et al. ((2015), (2016), (2017) Uzzaman
66 ((2012a), (2012b), (2012c), (2013))). However, this case may not fully represent the real
67 practice as the flanges are typically attached (fastened) to the supports. Such a flange
68 restraining has a significant impact on the web crippling failure of thin-walled members.
69 Bhakta et al. (1992) investigated the influence of flange restraints on the web crippling capacity
70 for conventional cold-formed steel members including channels (unlipped and lipped), I-
71 Sections, Z-Sections, hat sections, and floor decks. A total of fifty-two web crippling tests were
72 performed for fastened and unfastened member under EOF and IOF loading conditions.

73 Generally, it was found that restraining the flange makes a significant increase in the web
74 crippling capacity of the section. Gerges and Schuster (1998), Macdonald et al. (2011) and
75 Janarthanan et al. ((2015), (2019a), (2019b)) also carried out further experimental
76 investigations and proposed several improved equations to determine the web crippling
77 capacity for fastened cold-formed lipped channel steel beams under EOF and IOF loading
78 conditions. For two-flange loading conditions (ETF and ITF), Beshara and Schuster (2000)
79 reported the first experimental study in investigating the web crippling failure for fastened cold-
80 formed steel sections. A series of 72 tests were performed on both C and Z sections and
81 improved coefficients were established for fastened cold-formed steel sections under ETF and
82 ITF loading conditions, which were later adopted in the AS/NZS 4600 (2018) and AISI S100
83 (2016).

84 Very limited research has been undertaken to study the web crippling instability of
85 aluminium members. Tryland et al. (1999), Zhou and Young (2008), Young and Zhou (2008),
86 Zhou et al. (2009) Chen et al (2015) and Su and Young (2018) conducted experimental and
87 numerical studies on unfastened extruded aluminium hollow sections while Alsanat et al.
88 ((2019a), (2019b)) conducted experimental and numerical investigations on unfastened roll-
89 formed ALC sections under two-flange loading conditions. It should be noted that no
90 experimental data is available in the literature related to the web crippling mechanism of
91 fastened aluminium alloy sections.

92 This research, therefore, aims to study the web crippling mechanism of fastened ALC
93 sections under two-flange loading conditions. The tests were conducted on the same batch of
94 specimens reported by Alsanat et al. (2019a). Given the unavailability of specific and standard
95 web crippling testing methods for aluminium members, the specimen lengths and test set-up
96 were designed following the AISI S909 (2008) guidelines for cold-formed steel members. A

97 detailed assessment on the accuracy and reliability of the current web crippling design rules
98 provided by AS/NZS 1664.1 (1997), Aluminium design manual (AA 2015), AS/NZS 4600
99 (2018), AISI S100 (2016) and Eurocode 3 Part 1-3 (CEN 2006) was performed. As the
100 predictions from the aforementioned specifications were found unconservative and unreliable,
101 an improved design equation was then developed using a similar approach of the unified
102 equation given in AS/NZS 4600 (2018) to predict the web crippling capacity of fastened ALC
103 sections under two-flange load configurations. It should be noted that the web crippling design
104 guidelines specified in the AS/NZS 1664.1 (1997) and Aluminium design manual (AA 2015)
105 for aluminium structures are identical, and therefore only AS/NZS 1664.1 (1997) is considered
106 in this paper. Similarly, The AS/NZS 4600 (2018) and AISI S100 (2016) design rules for cold-
107 formed steel structures are identical, and hence only AS/NZS 4600 (2018) is examined herein.
108 Moreover, the experimental data obtained from this study and those from Alsanat et al.'s
109 (2019a) were used to explore the influence of flange attachment on the capacity and behaviour
110 of the web crippling failure. A new prediction approach was subsequently proposed to estimate
111 the increase of the web crippling capacity of restrained sections.

112 **CURRENT DESIGN RULES**

113 It is known that the nominal web crippling capacities of thin-walled sections can be
114 predicted using AS/NZS 1664.1 (1997) and Eurocode 9 (CEN 2007) for aluminium structures,
115 and AS/NZS 4600 (2018) and Eurocode 3 Part 1-3 (CEN 2006) for cold-formed steel structures.
116 However, the predictions of web crippling capacities using these specifications except AS/NZS
117 4600 (2018) are not differentiated between sections with fastened and unfastened support
118 conditions.

119 **AS/NZS Specifications**

120 *AS/NZS 1664.1 for Aluminium Members*

121 The web crippling design rules for thin-walled sections subjected to a concentrated
 122 transverse load are specified in the AS/NZS 1664 (1997) Part 1, Section 4.7.7 for aluminium
 123 structures. Equations (1) and (2) express the nominal web crippling capacity (P_{AS1664}) of ALC
 124 sections under the ETF and ITF loading conditions, respectively.

$$125 \quad P_{AS1664} = \frac{C_1 t^2 \sin \theta (0.46 f_y + 0.02 \sqrt{E f_y}) (N + C_{w2})}{C_{w3} + r_i (1 - \cos \theta)} \quad \text{(ETF)} \quad (1)$$

$$126 \quad P_{AS1664} = \frac{C_2 t^2 \sin \theta (0.46 f_y + 0.02 \sqrt{E f_y}) (N + C_{w1})}{C_{w3} + r_i (1 - \cos \theta)} \quad \text{(ITF)} \quad (2)$$

127 where $C_1 = 1.2$, $C_2 = 1.0$, $C_{w1} = 140\text{mm}$, $C_{w2} = 33\text{mm}$, $C_{w3} = 10\text{mm}$, t is the thickness of the web
 128 (mm), N is the bearing length (mm), r_i is the inside corner radius (mm), E is the elastic modulus
 129 (MPa), f_y is the static 0.2% yield stress (MPa), and θ is the angle between the web surface and
 130 the bearing surface plane. Note that θ is taken as 90° for the ALC sections used in this study.

131 Alsanat et al. (2019a) improved these equations to suitably predict the web crippling
 132 capacity of unfastened ALC sections under two-flange loading conditions. The effect of web
 133 slenderness was taken into consideration and the modified equations are:

$$134 \quad P_{AS1664 (Prop.)} = \frac{C_1 t^2 \sin \theta (0.46 f_y + 0.02 \sqrt{E f_y}) (N + C_{w2})}{C_{w3} + r_i (1 - \cos \theta)} \left(1 - C_{h1} \sqrt{\frac{h}{t}} \right) \quad \text{(ETF)} \quad (3)$$

$$135 \quad P_{AS1664 (Prop.)} = \frac{C_2 t^2 \sin \theta (0.46 f_y + 0.02 \sqrt{E f_y}) (N + C_{w1})}{C_{w3} + r_i (1 - \cos \theta)} \left(1 - C_{h2} \sqrt{\frac{h}{t}} \right) \quad \text{(ITF)} \quad (4)$$

136 where $C_1 = 0.31$, $C_2 = 258$, $C_{w1} = 780\text{mm}$, $C_{w2} = 238\text{mm}$, $C_{w3} = 10\text{mm}$, $C_{h1} = 0.05$ and $C_{h2} =$
 137 0.025 .

138 *AS/NZS 4600 for Cold-Formed Steel Members*

139 The AS/NZS 4600 (2018) provides a generalised design approach to estimate the web
 140 crippling capacity of various cold-formed steel sections. These sections include typical cold-
 141 formed steel sections including single web channels (lipped or unlipped), back-to-back channel
 142 sections, multi-web deck sections, single hat sections, and single web Z-sections. The unified
 143 Equation (5) given in the AS/NZS 4600 (2018) can be used to calculate the web crippling
 144 capacity (P_{AS4600}) of cold-formed steel members.

$$145 \quad P_{AS4600} = Ct^2 f_y \sin \theta \left(1 - C_R \sqrt{\frac{r_i}{t}}\right) \left(1 + C_N \sqrt{\frac{N}{t}}\right) \left(1 - C_h \sqrt{\frac{h}{t}}\right) \quad (5)$$

146 Where C , C_R , C_N is the coefficient of the bearing length and C_h is the coefficient of the
 147 slenderness of the web. The values of these coefficients are summarised in Table 1. Note that
 148 in Equation (5), the following conditions $h/t \leq 200$, $N/t \leq 210$, $r_i/t \leq 3$, $N/h \leq 2$, and $\theta =$
 149 90° must be satisfied.

150 Alsanat et al. (2019a) also modified this equation to accurately predict the web crippling
 151 capacity for unfastened ALC sections under the ETF and ITF loading conditions. The effect of
 152 elastic moduli of aluminium alloys was incorporated in the modified Equation (6), and the new
 153 coefficient factors (C , C_R , C_N and C_h) were proposed and given in Table 1.

$$154 \quad P_p = Ct^2 \sqrt{E f_y} \sin \theta \left(1 - C_R \sqrt{\frac{r_i}{t}}\right) \left(1 + C_N \sqrt{\frac{N}{t}}\right) \left(1 - C_h \sqrt{\frac{h}{t}}\right) \quad (6)$$

155

156 **Eurocode Specifications**

157 *Eurocode 9 for Aluminium Members*

158 The Eurocode 9 (CEN 2007) Part 1.4, Section 6.1.7.2 provides Equation (7) to predict
159 the web crippling capacity of roll-formed aluminium with unstiffened webs.

$$160 \quad P_{EC9} = \alpha t^2 \sqrt{f_y E} \left(2.4 + \left(\frac{\theta}{90} \right)^2 \right) \left(1 - 0.1 \sqrt{\frac{r_i}{t}} \right) \left(0.5 + \sqrt{\frac{0.02N}{t}} \right) \quad (7)$$

161 where α is the coefficient for various categories of local loads and support for multi-web
162 sections.

163 This equation follows the same approach of Equation (5) obtained from the AS/NZS
164 4600 (2018). However, it is only valid for multi-webs sections. Therefore, it is not considered
165 in this paper and the Eurocode 3 Part 1-3 (CEN 2006) will be evaluated instead.

166 *Eurocode 3 for Cold-formed Steel Members.*

167 The Eurocode 3 Part 1-3 (CEN 2006) provides several equations derived based on the
168 past experimental studies on cold-formed steel sections. Equations (8) and (9) are the design
169 formulae for unstiffened single-web sections under ETF and ITF loading conditions,
170 respectively.

$$171 \quad P_{EC3} = \frac{k_1 k_2 k_3 f_y t^2}{\gamma_{M1}} \left[6.66 - \frac{d_w}{64t} \right] \left[1 + 0.01 \frac{N}{t} \right] \quad (8)$$

$$172 \quad P_{EC3} = \frac{k_3 k_4 k_5 f_y t^2}{\gamma_{M1}} \left[21 - \frac{d_w}{16.3t} \right] \left[1 + 0.0013 \frac{N}{t} \right] \quad (9)$$

173 where $k_1 = 1.33 - \frac{f_y}{690.9}$; $k_2 = 1.15 - 0.15 \frac{r_i}{t}$ ($0.5 \leq k_5 \leq 1.0$); $k_3 = 0.7 + 0.3 \left(\frac{\theta}{90}\right)^2$;

174 $k_4 = 1.22 - \frac{f_y}{1036.4}$; $k_5 = 1.06 - 0.06 \frac{r_i}{t}$ ($k_5 \leq 1.0$); d_w is the web height between
175 flange mid-lines in mm; γ_{M1} is the partial safety factor ($\gamma_{M1} = 1$) and θ is taken as 90° . Not
176 that Equations (8) and (9) are limited for cold-formed steel sections with $d_w/t \leq 200$ and $r_i/t \leq 6$.

177

178 Taking into account the effect of elastic moduli of aluminium alloys, a slight
179 modification was made to Equations (8) and (9) by Alsanat et al. (2019a) to enhance their web
180 crippling predictions for unfastened ALC sections under two-flange loading conditions. The
181 modified Equations (10) and (11) are:

182
$$P_{EC3(Prop.)} = \frac{0.028k_1k_2k_3\sqrt{E}f_yt^2}{\gamma_{M1}} \left[6.66 - \frac{d_w}{64t}\right] \left[1 + 0.01 \frac{N}{t}\right] \quad (10)$$

183
$$P_{EC3(Prop.)} = \frac{0.034k_3k_4k_5\sqrt{E}f_yt^2}{\gamma_{M1}} \left[21 - \frac{d_w}{16.3t}\right] \left[1 + 0.0013 \frac{N}{t}\right] \quad (11)$$

184 **EXPERIMENTAL STUDY**

185 **Test Specimens**

186 The web crippling experimental tests comprising 40 specimens of ALC sections with
187 restrained flanges were performed in the structural laboratory at Griffith University. The test
188 specimens were fabricated using aluminium alloy grade 5052 H36. The channel sections had
189 five different sectional sizes, which are commonly used in aluminium structural systems. The
190 section depth (d) varied from 100 to 250 mm, and two nominal thicknesses (t) of 2.5 and 3 mm
191 were considered. The specimens were cut to specific lengths (L) according to AISI S909

192 (2008). The specimen length (L) is three times the clear web height ($3h$) for the ETF loading
193 condition, and $5h$ for the ITF loading condition. All the specimens geometrical dimensions
194 were accurately measured and summarised in Tables 2 and 3 for ETF and ITF, respectively

195 High-strength steel plates were used to apply the bearing load and to support the
196 specimens. Four bearing plates with different lengths ranged from 25 mm to 150 mm were used
197 to investigate the influence of bearing length on the web crippling capacity. During the test,
198 the specimen flanges were fastened to the bearing plates using a 12mm bolt per flange.

199 The specimens were labelled to easily identify the loading condition, web height and
200 thickness, and the bearing plate length. For instance, the label “ITF-10030-N50” indicates that
201 the specimen’s loading condition is ITF, the nominal web height is 100 mm, the web thickness
202 (t) is 3 mm and the bearing length (N) is 50 mm.

203 **Material Properties**

204 To investigate the material properties of the specimens, tensile coupon tests were
205 conducted for each untested section (10030, 15030, 20025, 20030 and 25025). Three coupons
206 per section were cut from the longitudinal direction of the upper, bottom and centre parts of
207 the flat portion of the web. The coupons were then tested according to AS 1391 (SA 2007) for
208 the material tensile testing. The material properties including the elastic modulus, yield stress,
209 ultimate stress and ultimate strain obtained from the tensile coupon tests are summarised in
210 Table 4. Figure 3 shows the typical stress-strain curve of structural aluminium alloy 5052 H36.

211 **Test Set-up and Procedure**

212 Forty tests were performed to investigate the web crippling mechanism of fastened
213 ALC sections under the ETF and ITF loading conditions. A compressive force was applied to
214 the specimens using the Materials Test System (MTS) machine with a compressive testing
215 capacity of 500kN. Figures 4 (a) to (c) show the test set-up for the ETF and ITF loading
216 conditions. High strength half-rounds were used at the bottom and the top of the specimen to
217 simulate a simply supported beam scenario.

218 The specimens were first positioned between two bearing plates with similar lengths at
219 the end and mid-span for both ETF and ITF loading conditions, respectively. Then, the flanges
220 were attached to the bearing plates using 12 mm bolts. The measuring load was initialised with
221 zero value and the test was then commenced. The cross-head of the MTS machine was driven
222 down at a constant rate of 2 mm/min until the specimen failure. The applied load and both
223 vertical and horizontal displacements of the ALC section were measured using a displacement
224 control system. As shown in Figure 4 (b), the lateral displacement were measured using three
225 laser displacement transducers (Lasers 1, 2 and 3) at three positions on the web, whereas the
226 vertical displacement of the top bearing plate was measured using Laser 4 as shown in Figures
227 4(a) and (c).

228 **TEST RESULTS AND DISCUSSION**

229 The experimental web crippling capacities ($P_{F-Exp.}$) acquired from the two series of tests
230 are presented in Tables 2 and 3. Note that the specimens ETF-10030-N50 and ITF-10030-N50
231 were both tested twice. 0.5% difference between the repeated tests was observed for ETF-
232 10030-N50 specimens and 1.0% difference was found for ITF-10030-N50 specimens,
233 signifying the accuracy and reliability of the test results.

234 **Web Crippling Behaviour**

235 Figures 5 (a) and (b) present the typical load-displacement responses for specimens
236 ETF-20025-N150 and ITF-15030-N150, respectively. The curves of Lasers 1, 2 and 3 represent
237 the lateral movements of the web in different longitudinal points while Laser 4 curve shows
238 the vertical deformation of the ALC section during the test. As shown in Figure 6, web crippling
239 failure was observed for all the ETF loading condition specimens. However, both web crippling
240 and flange crushing failures were witnessed in the tests of ITF loading condition. The
241 specimens loaded with 25 mm bearing plate experienced flange crushing failure as shown in
242 Figure 7 while those loaded with 50, 100 and 150 mm bearing plates failed in web crippling
243 failure (see Figure 8). Figure 9 (a) presents the applied load-vertical displacement responses
244 for the ITF-25025-N25 section, while the influence of the bearing length on the web crippling
245 failure capacities is illustrated in Figure 9 (b). The increased web crippling capacity for
246 specimens experiencing flange crushing is due to the significant reduction in the corner radii
247 of the deformed flange-web juncture and therefore the section became more resilient to the
248 applied concentrated load. Alsanat et al. (2019a), Gunalan and Mahendran (2015) and
249 Sundararajah et al. (2016) also observed a similar kind of failure during their experimental
250 works on unfastened channel sections. It should be mentioned that this study does not consider
251 the web crippling capacities obtained from the flange crushing tests when proposing design
252 rules.

253 **Specimen Length**

254 Alsanat et al. (2019a) found that the ITF specimens loaded with 100 mm and 150 mm
255 bearing plates were failed before reaching their maximum possible web crippling capacity due
256 to the short length of the specimens. This was evidenced from the deformation of the specimen
257 ends before reaching the maximum capacity of the sections. Alsanat et al. (2019b) numerically

258 investigated the influence of specimen length on the ultimate web crippling capacity of the
259 section by conducting an extensive parametric study. Figure 10 shows the load-vertical
260 displacement responses for unfastened ITF-25025-N150 specimen with different lengths ($L =$
261 5d, 6d, 9d and 13d). A significant drop of the 5d curve was observed comparing with 6d, 9d,
262 and 13d curves. Hence, it was recommended to increase the minimum specimen length to six
263 times the section height for any future web crippling studies using aluminium sections.
264 Similarly, in the current experimental study, it was found that the same specimens were also
265 slightly failed prematurely even though the flanges were fastened to the supports. Figure 9 (b)
266 shows the reduction in the capacities for the specimens loaded by 150 bearing length due to the
267 short in specimen's length. This specifies that the specimen length (L) recommended by the
268 AISI S909 (2008) should also be extended to 6d for the fastened ALC sections under the ITF
269 loading condition.

270 **The effect of restrained flanges**

271 To investigate the effect of restrained flanges on the web crippling capacity,
272 experimental data acquired from the present tests and those from Alsanat et al's (2019a)
273 experiments for unfastened sections were analysed. It was observed that restraining the flanges
274 has a considerable influence on the web crippling capacity of the ALC sections. In the case of
275 unrestrained flanges, the out-of-plane bending moment (M_1) acting on the web plate due to the
276 eccentric load (P_1) led to a large rotation to both the web and flanges, as shown in Figures 11
277 (a) and (b). Restraining the flanges, on the other hand, led to a significant reduction in M_1 due
278 to the initiation of the opposite load (P_2) and moment (M_2) generated from the bolts, which
279 eventually resulted in a substantial increase in the load carrying capability of the section as
280 shown in Figures 11 (c) and (d). Figures 12 (a) to (d) display the differences in the experimental

281 web crippling failure modes for fastened and unfastened specimens under ETF and ITF loading
282 conditions, respectively.

283 Figures 13 (a) and (b) compare the load-deflection curves for fastened and unfastened
284 cases for ETF-20030N100 and ITF-20025N150 specimens, respectively. The overall
285 behaviour is reasonably similar in both cases. Specifically, the displacement increased linearly
286 with the load at a different slope up to the maximum load, and the ultimate failure in both cases
287 practically occurred at the same vertical displacement. The maximum loads for the ETF-
288 20030N100 specimens under fastened and unfastened conditions are 8.64 kN and 5.82 kN,
289 respectively, with 33% difference while these values are 16.52 kN and 12.27 kN with 26%
290 difference for the ITF-20025N150 specimens.

291 Figures 14 (a) and (b) present the web crippling capacity ratios of the fastened and
292 unfastened sections under ETF and ITF loading conditions, respectively. Generally, it was
293 noticed that fastening the flanges resulted in a significant increase in the web crippling capacity
294 of the sections under both cases. Flange restraining had a more significant impact on the
295 sections under the ETF loading conditions with up to 82% more capacity with an average of
296 50%, however; for the ITF loading conditions, the capacity increased to 40% with an average
297 of 16%.

298 **DESIGN RULES**

299 **Comparison of Test Results with Current Design Rules**

300 The web crippling capacities obtained from the experimental results of the specimens
301 with flanges being restrained were compared with the design capacities predicted by the
302 AS/NZS 1664.1 (1997) for aluminium structures, and AS/NZS 4600 (2018) and Eurocode 3

303 Part 1-3 (CEN 2006) for cold-formed steel structures. As mentioned earlier, the equations given
304 by both AS/NZS 1664.1 (1997) and Eurocode 3 Part 1-3 (CEN 2006) are not differentiated
305 between unfastened and fastened support conditions. Therefore their predictions are identical
306 in both cases even though the experimental web crippling capacities with fastened and
307 unfastened flanges are significantly different.

308 Tables 5 and 6 show the comparisons of the test strengths (P_{F-Exp}) with the design
309 capacities predicted using the AS/NZS 1664.1 (1997) (P_{AS1664}), AS/NZS 4600 (2018) (P_{AS4600})
310 and Eurocode 3 Part 1-3 (CEN 2006) (P_{EC3}) for the ETF and ITF loading conditions,
311 respectively. The average measured cross-section dimensions and the measured material
312 properties as given in Tables 2-4 were used to calculate the design strengths of the test
313 specimens. For the loading condition of ETF with restrained flanges, the mean values of test-
314 to-predicted strength ratios P_{F-Exp}/P_{AS1664} , P_{F-Exp}/P_{AS4600} and P_{F-Exp}/P_{EC3} are 0.73, 0.72 and 0.74,
315 with the corresponding COVs of 0.24, 0.11 and 0.092, respectively. For the fastened specimens
316 under the loading condition of ITF, the mean values of P_{F-Exp}/P_{AS1664} , P_{F-Exp}/P_{AS4600} and P_{F-}
317 Exp/P_{EC3} are 1.03, 0.66 and 0.72 with the corresponding COVs values of 0.15, 0.05 and 0.11,
318 respectively. Generally, it is found that the predicted web crippling strengths using the currently
319 available design rules are unconservative for both loading conditions, except for the capacities
320 predicted by the AS/NZS 1664.1 (1997) specification under the ITF load case, with a
321 reasonably acceptable mean value but an unreliable COV value. Therefore, accurate design
322 rules are needed to predict the web crippling capacities of fastened ALC sections under two-
323 flange loading conditions.

324 **Modified Design Rules**

325 The modified design equation presented in this study follows the same approach
326 obtained from the AS/NZS 4600 (2018). This is due to the fact that: (i) this generalised
327 approach is the only available one for both fastened and unfastened cases, (ii) it is also
328 employed by other specifications, e.g. Eurocode 9 Part 1-4 (CEN 2007) and AISI S100 (2016),
329 and (iii) it is suitable for both cold-formed steel and aluminium members as confirmed by
330 Alsanat et al. (2019a). Table 1 summarises the proposed coefficients (C , C_R , C_N and C_h)
331 associated with Equation (6) to predict the web crippling capacity of fastened ALC sections
332 under two-flange loading conditions.

333 The web crippling strengths, predicted by Equation (6) implementing the proposed web
334 crippling coefficients, agree well with the experimental results of fastened ALC sections under
335 the ETF and ITF loading conditions, as evidenced in Tables 5 and 6. The mean value of test-
336 to-predicted capacity ratios of the specimens under the ETF loading condition is 1.00 with a
337 COV of 0.08 while these values are 1.01 and 0.04 for the ITF loading conditions. Figures 15
338 (a) and (b) show the comparison between the experimental web crippling capacities of the ALC
339 sections with the predictions using the proposed equation under the ETF and ITF loading
340 conditions, respectively; from which the suitability of the proposed equation is confirmed.

341 **Proposed Design Rules Incorporating Flange Fastening Effect**

342 To propose a reliable approach to predict the increase of the web crippling capacities
343 of fastened sections, the effect of restraining flanges on the main web crippling parameters
344 should be first investigated. Figures 16 (a) and (b) were plotted for the ETF and ITF loading
345 conditions, respectively, to demonstrate the relationship between the web crippling capacity
346 ratios (P_F/P_U) against the bearing length to thickness ratios (N/t) for web slenderness ratios

347 (h/t) ranging from 30 to 101. Increasing the bearing length to thickness ratios (N/t) leads to an
348 increase in the capacity ratio (P_F/P_U) due to flange restraint. However, such an elevation
349 reduces when the web slenderness (h/t) increases. For instance, the rising slope of the ETF
350 specimens with the web slenderness (h/t) of 30 is 0.016, while the slope drops to 0.004 for the
351 ETF specimens with h/t of 101. Therefore, it can be concluded that both the bearing length to
352 thickness (N/t) and the web slenderness (h/t) ratios have a compound flange restraining effect
353 on the web crippling capacity of aluminium lipped channel sections.

354 From this observation, the influence of fastening the flanges on the web crippling
355 capacity of the ALC sections (P_F/P_U), was plotted against the geometrical factor Nh/t^2 for the
356 ETF and ITF loading conditions in Figures 17 (a) and (b), respectively. It was observed that by
357 increasing the Nh/t^2 factor, the effect of flange fastening increases considerably in a nonlinear
358 manner. Using non-linear least-squares to curve fit the data in Figures 17 (a) and (b), a new
359 equation was proposed to predict the increase on the web crippling capacity due to flange
360 restraint.

361
$$K_F = 0.6 \left(\frac{Nh}{t^2} \right)^a \geq 1 \quad (12)$$

362 where K_F is the fastening factor, the coefficients $a = 0.126$ and 0.095 for the ETF and ITF
363 loading conditions, respectively.

452 This equation can be used in conjunction with any web crippling design rules for
453 unfastened lipped channel sections to predict the increased web crippling capacity for fastened
454 sections. The modified web crippling equations reported by Alsanat et al. (2019a) (Equations
455 (3), (4), (6), (10) and (11)) for unfastened ALC sections under two-flange loading conditions
456 were used in this study to assess the accuracy and reliability of the proposed fastening factor.

457 Tables 5 and 6 give the ratios of the test results to the predictions of Alsanat et al.'s (2019a)
 458 modified equations multiplied by the fastening factor (k_F). For the ETF loading condition
 459 (modified Equations (3), (6) and (10) multiplied by the K_F), the mean values of the test-to-
 460 predicted web crippling capacities of fastened ALC sections are 1.00, 1.00 and 0.99 while the
 461 corresponding COV values are 0.05, 0.08 and 0.07, respectively. For the ITF loading condition
 462 (modified Equations (4), (6) and (11) multiplied by the K_F), the mean values are 1.00, 1.01 and
 463 0.98 and the corresponding COV values are 0.04, 0.03 and 0.03, respectively. It can be
 464 concluded that the web crippling capacity formulae incorporating the fastening factor is able
 465 to accurately predict the increased capacities of the ALC sections under two-flange loading
 466 conditions when the flanges are restrained to the supports (see Figures 15(a) and (b)).

467 **Capacity Reduction Factor (ϕ_w)**

468 The capacity reduction factor (ϕ_w) can be determined using the statistical model
 469 specified in the AISI S100 (2016) specification. This model considers various fabrication,
 470 material, and loading effects. Equation (13) is generally used to determine the capacity
 471 reduction factor for the capacity ratios gained from the international specifications and the
 472 proposed design rules.

$$473 \quad \phi_w = 1.5M_m F_m P_m e^{-\beta_0 \sqrt{V_M^2 + V_F^2 + C_n V_P^2 + V_Q^2}} \quad (13)$$

474 where ϕ_w is the resistance factor; $M_m = 1.1$ and $V_m = 0.06$ are respectively the mean and
 475 coefficient of variation of the material factor; $\beta_0 = 2.5$ is the target reliability index for beams;
 476 $F_m = 1.0$ and $V_F = 0.05$ are respectively the mean and coefficient of variation of the fabrication
 477 factor r ; $C_n = \frac{n^2-1}{n^2-3n}$ is the correction factor depending on the number of tests; $V_Q = 0.21$ is
 478 the coefficient of variation of load effect; P_m is the mean value of the test-to-predicted load

479 ratios; V_p is the coefficient of variation of the test-to-predicted load ratios and n is the number
480 of tests.

481 Tables 5 and 6 show the capacity reduction factors (ϕ_w) for the proposed design rules.
482 They are ranging between 0.90 and 0.94 and thus it is suggested to consider a ϕ_w factor of 0.90
483 for all the proposed design rules to estimate the web crippling capacities of the ALC sections
484 under the two-flange loading conditions.

485 CONCLUSIONS

486 This paper described the details of an experimental investigation of fastened roll-
487 formed aluminium lipped channel (ALC) sections under web crippling action with End-Two-
488 Flange (ETF) and Interior-Two-Flange (ITF) loading conditions. Forty tests were performed
489 with different geometrical cross-section parameters and bearing lengths. The details of web
490 crippling results in terms of ultimate loads, load-deformation responses, and failure modes
491 were discussed in detail. Web crippling is the prominent failure for both loading conditions
492 however, the ITF specimens loaded with 25 mm bearing plates experienced a combined flange
493 crushing and web crippling failure. Comparisons with the experimental results of fastened ALC
494 sections showed that the nominal web crippling capacities predictions of the design guidelines
495 obtained from the AS/NZS 1664.1 (1997), AS/NZS 4600 (2018) and Eurocode 3 Part 1-3 (CEN
496 2006) are mostly unconservative and unreliable. Hence, a modified design rule was proposed
497 based on the experimental results to precisely predict the ultimate web crippling capacities of
498 fastened ALC sections. Furthermore, the effect of restrained flanges on the web crippling
499 capacity was discussed in detail. Fastening the flanges led to a significant increase in the web
500 crippling capacity of the sections under both loading conditions (up to 82% more capacity for
501 the ETF load case, and 40% for the ITF load case). A new design approach, incorporating the

502 fastening factor (k_f), was developed in this paper to predict the increased web crippling capacity
503 due to fastened flanges. The results showed that this novel approach can be used in conjunction
504 with the unfastened web crippling design guidelines to estimate the capacities of fastened ALC
505 sections.

506 **ACKNOWLEDGEMENTS**

507 The authors wish to thank Griffith University for providing the necessary test facilities
508 and technical support, and to Mr Robert Price from BlueScope Building Components Pty Ltd
509 for supplying the test specimens.

510 **REFERENCES**

511 AISI (American Iron and Steel Institute). (2008). “Standard test method for determining the
512 web crippling strength of cold-formed steel beams.” AISI S909, Washington, DC.

513 AISI (American Iron and Steel Institute). (2016). “Specifications for the cold-formed steel
514 structural members, cold-formed steel design manual.” AISI S100, Washington, DC.

515 Alsanat, H., Gunalan, S., Guan, H., Poologanathan, K, and Bull, J. (2019a). “Experimental
516 study of aluminium lipped channel sections subjected to web crippling under two-
517 flange load cases.” *Thin-Walled Struct.*, 141, 460-476.

518 Alsanat, H., Gunalan, S., Guan H., Poologanathan K. and Tsavdaridis K. D. (2019b). “Web
519 crippling behaviour and design for aluminium lipped channel sections under two-
520 flange loading conditions.” *Thin-Walled Struct.*, In press.

521 Aluminium Association (AA) (2015), Aluminium design manual, Washington, D.C.

522 AS (Australian Standard). (2007), “Methods for tensile testing of metal.” *AS 1391*, Sydney,
523 Australia.

524 AS/NZS (Australian/New Zealand Standard). (1997). “Aluminum structures part 1: Limit state
525 design.” *AS/NZS 1664.1*, Sydney, Australia

526 AS/NZS (Australian/New Zealand Standard). (2018). “Cold-formed steel structures.” *AS/NZS*
527 *4600*, Sydney, Australia.

528 Beshara, B., and Schuster, R. M. (2000). “Web crippling of cold formed steel C- and Z-
529 sections.” *Proc., 15th Int. Specialty Conf. on Cold-Formed Steel Structures*,
530 Department of Civil Engineering Center for Cold- Formed Steel Structures, Rolla,
531 MO.

532 Bhakta, B. H., LaBoube, R. A., and Yu, W. W. (1992). “The effect of flange restraint on web
533 crippling strength.” *Civil Engineering Study 92-1, Cold-Formed Steel Series, Final*
534 *Rep.*, Univ. of Missouri-Rolla, Rolla, Mo

535 CEN (European Committee for Standardization). (2006). “Eurocode 3: Design of steel
536 structures—Part 1-3: General rules—Supplementary rules for cold-formed members
537 and sheeting.” *EN 1993-1-3*, Brussels, Belgium.

538 CEN (European Committee for Standardization). (2007). “Eurocode 9: Design of aluminum
539 structures—Part 1-4: Cold-formed structural sheeting.” *EN 1999-1-1*, Brussels,
540 Belgium.

541 Chen, Y., Chen, X., and Wang, C. (2015). “Aluminium tubular sections subjected to web
542 crippling.” *Thin-Walled Struct.*, 90, 49-60.

543 Gerges, R. R., and Schuster, R. M. (1998). "Web crippling of single web cold-formed steel
544 members subjected to end one-flange loading." *Proc., 14th Int. Specialty Conf. on*
545 *Cold-Formed Steel Structures*, Univ. of Missouri, Rolla, MO.

546 Gunalan, S., and Mahendran, M. (2015). "Web crippling tests of cold-formed steel channels
547 under two-flange load cases." *J. Constr. Steel Res.*, 110, 1–15.

548 Gunalan, S., and Mahendran, M. (2019). "Experimental study of unlipped channel beams
549 subject to web crippling under one flange load cases." *Adv. Steel Constr.*, 15(2), 165-
550 72.

551 Islam, S. Z., and Young, B. (2018). "Design of CFRP-strengthened aluminium alloy tubular
552 sections subjected to web crippling." *Thin-Walled Struct.*, 124, 605-621.

553 Janarthanan, B., Mahendran, M., and Gunalan, S. (2015). "Bearing capacity of cold-formed
554 unlipped channels with restrained flanges under EOF and IOF load cases." *Steel*
555 *Constr.*, 8(3), 146-154.

556 Janarthanan, B., Mahendran, M., and Gunalan, S. (2019a). "Numerical modelling of web
557 crippling failures in cold-formed steel unlipped channel sections." *J. Constr. Steel*
558 *Res.*, 158, 486-501.

559 Janarthanan, B., Sundararajah, L., Mahendran, M., Keerthan, P., and Gunalan, S. (2019b).
560 "Web crippling behaviour and design of cold-formed steel sections." *Thin-Walled*
561 *Struct.*, 140, 387-403.

562 Keerthan, P., and Mahendran, M. (2014). "Experimental study of web crippling behaviour of
563 hollow flange channel beams under two-flange load cases." *Thin-Walled Struct.*, 85,
564 207–219.

565 Keerthan, P., and Mahendran, M. (2016). "Experimental study on web crippling strength of
566 hollow flange channels under end-one-flange and interior-one-flange load cases."
567 *Adv. in Struct. Eng.*, 19(6), 966-981.

568 Macdonald, M., Heiyantuduwa, M. A., Kotelko, M., and Rhodes, J. (2011). "Web crippling
569 behavior of thin-walled lipped channel beams." *Thin-Walled Struct.*, 49(5), 682–690.

570 Steau, E., Mahendran, M., and Keerthan, P. (2015). "Web crippling tests of rivet fastened
571 rectangular hollow flange channel beams under two-flange load cases." *Thin-Walled
572 Struct.*, 95, 262-275.

573 Steau, E., Keerthan, P., and Mahendran, M. (2016). "Web crippling capacities of rivet
574 fastened rectangular hollow flange channel beams under one-flange load cases." *Steel
575 Constr.*, 9(3), 222-239.

576 Steau, E., Keerthan, P., and Mahendran, M. (2017). "Web crippling study of rivet fastened
577 rectangular hollow flange channel beams with flanges fastened to supports." *Adv. in
578 Struct. Eng.*, 20(7), 1059-1073.

579 Su, M. N., and Young, B. (2018). "Design of aluminium alloy stocky hollow sections
580 subjected to concentrated transverse loads." *Thin-Walled Struct.*, 124, 546-557.

581 Sundararajah, L., Mahendran, M., and Keerthan, P. (2016). "Experimental studies of lipped
582 channel beams subject to web crippling under two-flange load cases." *J. Struct. Eng.*,
583 [10.1061/\(ASCE\)ST.1943-541X.0001523](https://doi.org/10.1061/(ASCE)ST.1943-541X.0001523).

584 Sundararajah, L., Mahendran, M., and Keerthan, P. (2017). "New design rules for lipped
585 channel beams subject to web crippling under two-flange load cases." *Thin-Walled
586 Struct.*, 119(2), 421–437.

587 Tryland, B. T., Langseth, M., and Hopperstad, O. S. (1999). “Nonperfect aluminum beams
588 subjected to concentrated loading.” *J. Struct. Eng.*, 125(8), 900–909.

589 Uzzaman, A., Lim, J. B. P., Nash, D., Rhodes, J., and Young, B. (2012a). “Cold-formed steel
590 sections with web openings subjected to web crippling under two-flange loading
591 conditions—Part I: Tests and finite element analysis.” *Thin-Walled Struct.*, 56, 38–48.

592 Uzzaman, A., Lim, J. B. P., Nash, D., Rhodes, J., and Young, B. (2012b). “Cold-formed steel
593 sections with web openings subjected to web crippling under two-flange loading
594 conditions—Part II: Parametric study and proposed design equations.” *Thin-Walled
595 Struct.*, 56, 79–87.

596 Uzzaman, A., Lim, J. B. P., Nash, D., Rhodes, J., and Young, B. (2012c). “Web crippling
597 behaviour of cold-formed steel channel sections with offset web holes subjected to
598 interior-two-flange loading.” *Thin-Walled Struct.*, 50(1), 76–86.

599 Uzzaman, A., Lim, J. B. P., Nash, D., Rhodes, J., and Young, B. (2013). “Effect of offset web
600 holes on web crippling strength of cold-formed steel channel sections under end-two-
601 flange loading condition.” *Thin-Walled Struct.*, 65, 34–48.

602 Young, B., and Hancock, G. J. (2001). “Design of cold-formed channels subjected to web
603 crippling.” *J. Struct. Eng.*, 10.1061/(ASCE)0733-9445(2001)127:10(1137), 1137–
604 1144.

605 Young, B., and Zhou, F. (2008). “Aluminium tubular sections subjected to web crippling—
606 Part II: Proposed design equations.” *Thin-Walled Struct.*, 46(4), 352-361.

607 Zhou, F., and Young, B. (2008). “Aluminium tubular sections subjected to web crippling—
608 Part I.” *Thin-Walled Struct.*, 46(4), 339-351.

609 Zhou, F., Young, B., and Zhao, X.L. (2009). "Tests and design of aluminium tubular sections
610 subjected to concentrated bearing load." *J. Struct. Eng.*, [10.1061/\(ASCE\)ST.1943-](https://doi.org/10.1061/(ASCE)ST.1943-541X.0000015)
611 [541X.0000015](https://doi.org/10.1061/(ASCE)ST.1943-541X.0000015).

612

613

Table 1. AS/NZS 4600 and proposed coefficients for lipped channel sections.

Equation	Flange condition	Load case	C	C_R	C_N	C_h	ϕ_w
Current (AS/NZS 4600)	Fastened	ETF	7.5	0.08	0.12	0.048	0.85
		ITF	20	0.10	0.08	0.031	0.85
Alsanat et al. (2019a)	Unfastened	ETF	0.273	0.21	0.16	0.06	0.90
		ITF	0.78	0.17	0.04	0.03	0.93
Proposed	Fastened	ETF	0.231	0.21	0.35	0.05	0.91
		ITF	0.78	0.20	0.08	0.02	0.93

Table 2. Specimen details and test results for fastened ETF load case.

Specimen	Depth d (mm)	Thickness t (mm)	Radius r_i (mm)	Flange b_f (mm)	Lip l_b (mm)	Length L (mm)	Load $P_{F-Exp.}$ (kN)
ETF-10030-N25	107.2	2.95	4.9	60.5	14.8	316	6.80
ETF-10030-N50(a)	106.4	2.95	5.0	58.3	16.2	317	8.46
ETF-10030-N50(b)	107.2	2.97	4.9	59.6	15.0	317	8.42
ETF-10030-N100	107.2	2.95	4.8	59.3	15.1	316	11.25
ETF-15030-N25	156.8	2.93	4.9	62.9	23.0	466	6.37
ETF-15030-N50	157.6	2.93	5.0	63.2	22.3	465	7.84
ETF-15030-N100	158.4	2.92	5.1	63.3	21.8	465	9.92
ETF-15030-N150	155.4	2.92	4.9	63.4	23.0	467	12.45
ETF-20025-N25	208.2	2.42	5.1	74.5	25.4	617	4.74
ETF-20025-N50	208.0	2.43	4.9	74.3	25.3	615	5.15
ETF-20025-N100	207.2	2.43	5.0	74.2	25.8	615	6.19
ETF-20025-N150	204.1	2.43	4.8	75.9	26.4	615	7.51
ETF-20030-N25	204.5	2.9	4.6	74.9	27.5	611	6.45
ETF-20030-N50	208.3	2.9	5.0	73.1	27.6	615	7.37
ETF-20030-N100	204.4	2.89	4.6	75.5	27.6	613	8.64
ETF-20030-N150	208.2	2.89	5.0	73.4	27.2	615	11.05
ETF-25025-N25	259.9	2.43	4.4	80.7	23.5	765	4.45
ETF-25025-N50	259.8	2.44	4.9	76.2	23.8	765	4.90
ETF-25025-N100	262.2	2.44	4.8	76.1	22.6	765	6.20
ETF-25025-N150	260.4	2.45	4.6	76.2	23.5	765	7.20

Note: ETF-10030-N50(a) and ETF-10030-N50(b) were repeated tests

Table 3. Specimen details and test results for fastened ITF load case.

Specimen	Depth d (mm)	Thickness t (mm)	Radius r_i (mm)	Flange b_f (mm)	Lip l_b (mm)	Length L (mm)	Load $P_{F-Exp.}$ (kN)
ITF-10030-N25	106.8	2.94	4.8	59.3	14.3	527	21.88
ITF-10030-N50(a)	106.5	2.95	4.9	59.4	14.8	525	20.69
ITF-10030-N50(b)	106.8	2.94	4.9	59.0	14.4	521	20.90
ITF-10030-N100	106.2	2.94	4.8	59.6	14.4	523.5	23.68
ITF-15030-N25	156.6	2.93	4.8	62.6	22.6	774	19.99
ITF-15030-N50	156.8	2.92	4.9	62.4	22.7	775	19.34
ITF-15030-N100	156.3	2.92	4.8	62.1	22.7	776	22.99
ITF-15030-N150	156.7	2.93	4.9	62.5	22.8	774	23.99
ITF-20025-N25	206.3	2.43	4.6	74.0	26.3	1028	13.41
ITF-20025-N50	207.3	2.44	4.9	73.3	26.0	1022	13.93
ITF-20025-N100	207.4	2.43	5.0	73.9	26.3	1019	15.83
ITF-20025-N150	207.5	2.44	4.6	73.4	26.9	1021	16.52
ITF-20030-N25	205.5	2.9	4.4	74.5	31.6	1022	19.46
ITF-20030-N50	206.7	2.93	4.8	75.3	27.4	102	19.97
ITF-20030-N100	206.4	2.9	4.8	74.4	26.7	1021	22.63
ITF-20030-N150	206.6	2.89	4.6	74.5	26.7	1022	22.67
ITF-25025-N25	259.8	2.43	4.4	76.1	22.1	1273	14.21
ITF-25025-N50	260.1	2.42	4.5	76.0	22.4	1274	14.05
ITF-25025-N100	259.9	2.43	4.5	76.3	22.5	1269	15.99
ITF-25025-N150	259.8	2.43	4.5	76.2	22.2	1275	16.72

Note: ITF-10030-N50(a) and ITF-10030-N50(b) were repeated tests

Table 4. Mechanical properties of aluminium sections used in the experimental study.

Section	E (GPa)	$\sigma_{0.2}$ (MPa)	σ_u (MPa)	ε_u (%)
10030	65.05	210	259	6.15
15030	63.55	206	248	5.55
20025	63.95	214	260	5.05
20030	64.13	212	257	6.47
25025	64.34	216	265	6.68

Note: E = elastic modulus, $\sigma_{0.2}$ = static 0.2% tensile proof stress, σ_u = tensile strength and ε_u = ultimate strain

Table 5. Experimental ultimate loads and comparisons with current and proposed design rules – fastened ETF load case.

Specimen	h/t	$P_{F-Exp.}$ (kN)	Ultimate load ratios (Test-to-predicted)						
			P_{AS1664}	P_{AS4600}	P_{EC3}	$K_F \cdot P_{U-AS1664}$	$K_F \cdot P_{U-AS4600}$	$K_F \cdot P_{U-EC3}$	P_P
F-ETF-10030-N25	31.1	6.80	0.98	0.56	0.61	0.96	0.90	0.94	0.86
F-ETF-10030-N50	30.7	8.44	0.86	0.63	0.70	1.00	0.91	1.00	0.89
F-ETF-10030-N100	31.1	11.25	0.70	0.73	0.81	1.03	0.94	1.05	0.94
F-ETF-15030-N25	48.1	6.37	0.95	0.59	0.61	0.97	0.94	0.92	0.92
F-ETF-15030-N50	48.4	7.84	0.82	0.66	0.70	1.01	0.94	0.97	0.94
F-ETF-15030-N100	48.7	9.92	0.66	0.74	0.79	1.01	0.95	1.00	0.97
F-ETF-15030-N150	47.9	12.45	0.59	0.85	0.86	1.03	1.01	1.04	1.05
F-ETF-20025-N25	79.8	4.74	1.02	0.72	0.76	1.13	1.17	1.13	1.16
F-ETF-20025-N50	79.6	5.15	0.76	0.69	0.73	1.00	1.01	1.00	1.01
F-ETF-20025-N100	79.2	6.19	0.57	0.73	0.76	0.94	0.95	0.95	0.97
F-ETF-20025-N150	78.0	7.51	0.50	0.80	0.78	0.93	0.96	0.93	1.01
F-ETF-20030-N25	65.3	6.45	0.94	0.65	0.64	1.01	1.03	0.97	1.01
F-ETF-20030-N50	66.4	7.37	0.77	0.68	0.70	1.00	0.97	0.96	0.98
F-ETF-20030-N100	65.6	8.64	0.59	0.74	0.74	0.94	0.94	0.94	0.96
F-ETF-20030-N150	66.6	11.05	0.53	0.82	0.81	0.97	0.99	0.98	1.03
F-ETF-25025-N25	101.3	4.45	0.90	0.73	0.71	1.07	1.19	1.07	1.16
F-ETF-25025-N50	100.5	4.90	0.71	0.72	0.73	1.01	1.07	1.01	1.05
F-ETF-25025-N100	101.5	6.20	0.55	0.79	0.78	0.99	1.05	1.00	1.06
F-ETF-25025-N150	100.4	7.20	0.46	0.83	0.78	0.93	1.02	0.94	1.05
Mean			0.73	0.72	0.74	1.00	1.00	0.99	1.00
COV			0.24	0.11	0.09	0.05	0.08	0.05	0.08
ϕ_w						0.92	0.90	0.92	0.91

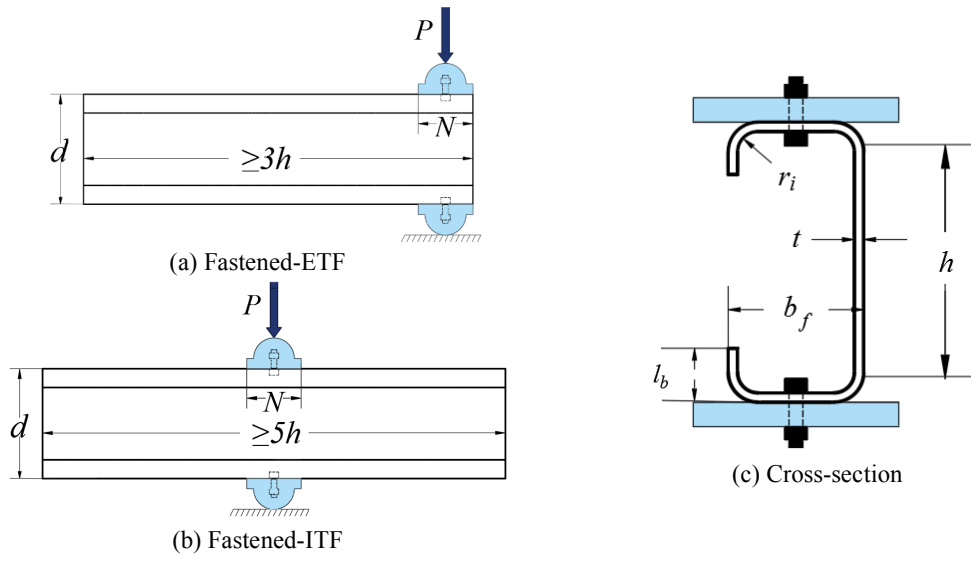
Table 6. Experimental ultimate loads and comparisons with current and proposed design rules - fastened ITF load case.

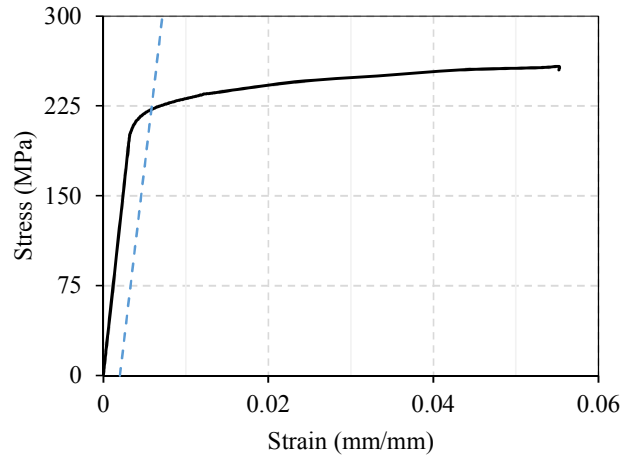
Specimen	h/t	$P_{F-Exp.}$ (kN)	Ultimate load ratios (Test/Prediction)						
			P_{AS1664}	P_{AS4600}	P_{EC3}	$K_F \times$ $P_{U-AS1664}$	$K_F \times$ $P_{U-AS4600}$	$K_F \times$ P_{U-EC3}	P_P
ITF-10030-N25	31.1	21.88 ^a	1.33	0.68	0.65	-	-	-	-
ITF-10030-N50	30.8	20.79	1.10	0.59	0.60	1.04	1.00	0.97	0.94
ITF-10030-N100	30.9	23.68	0.99	0.62	0.68	1.04	1.02	1.02	0.98
ITF-15030-N25	48.2	19.99 ^a	1.25	0.67	0.64	-	-	-	-
ITF-15030-N50	48.3	19.34	1.06	0.61	0.62	1.00	0.98	0.93	0.95
ITF-15030-N100	48.2	22.99	0.99	0.65	0.72	1.05	1.03	1.01	1.01
ITF-15030-N150	48.1	23.99 ^b	0.86	0.63	0.73	1.00	0.99	0.99	0.99
ITF-20025-N25	79.0	13.41 ^a	1.17	0.68	0.69	-	-	-	-
ITF-20025-N50	78.9	13.93	1.06	0.65	0.71	1.00	1.02	0.95	1.01
ITF-20025-N100	79.2	15.83	0.97	0.67	0.79	1.02	1.03	1.00	1.05
ITF-20025-N150	79.2	16.52 ^b	0.81	0.64	0.79	0.94	0.97	0.96	0.99
ITF-20030-N25	65.9	19.46 ^a	1.18	0.67	0.66	-	-	-	-
ITF-20030-N50	65.3	19.97	1.05	0.63	0.66	1.00	1.00	0.94	0.97
ITF-20030-N100	65.9	22.63	0.97	0.66	0.75	1.02	1.02	1.00	1.02
ITF-20030-N150	66.3	22.67 ^b	0.80	0.62	0.73	0.93	0.95	0.94	0.96
ITF-25025-N25	101.3	14.21 ^a	1.21	0.74	0.79	-	-	-	-
ITF-25025-N50	101.7	14.05	1.05	0.69	0.78	1.01	1.05	0.98	1.04
ITF-25025-N100	101.2	15.99	0.94	0.70	0.85	1.00	1.04	1.01	1.06
ITF-25025-N150	101.3	16.72 ^b	0.81	0.68	0.87	0.96	1.00	0.99	1.03
Mean			1.03	0.66	0.72	1.00	1.01	0.98	1.00
COV			0.15	0.05	0.11	0.04	0.03	0.03	0.04
ϕ_w						0.93	0.94	0.92	0.93

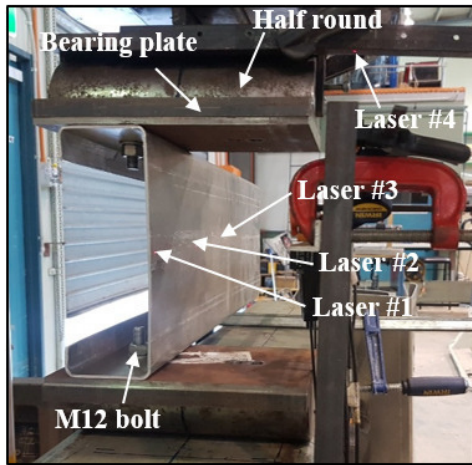
Note: ^a The specimen failed in combined web crippling and flange crushing.

^b The ends of specimen started to deform before reaching the ultimate load.

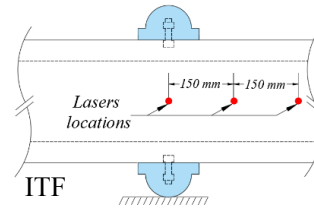
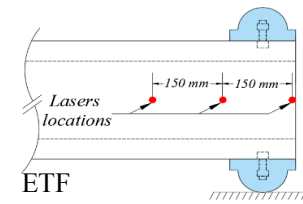




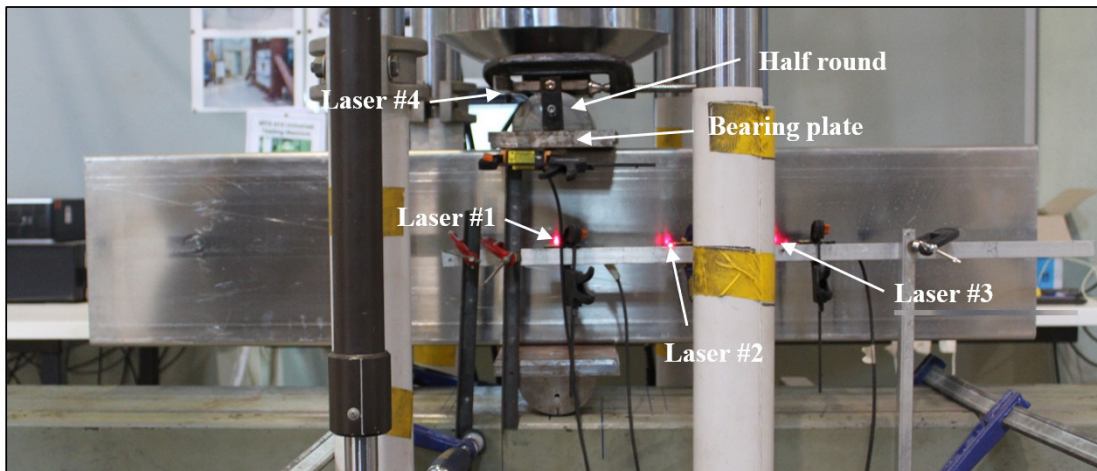




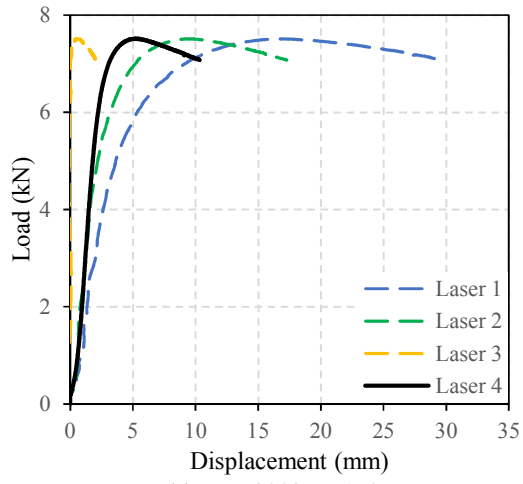
(a) Fastened ETF load case



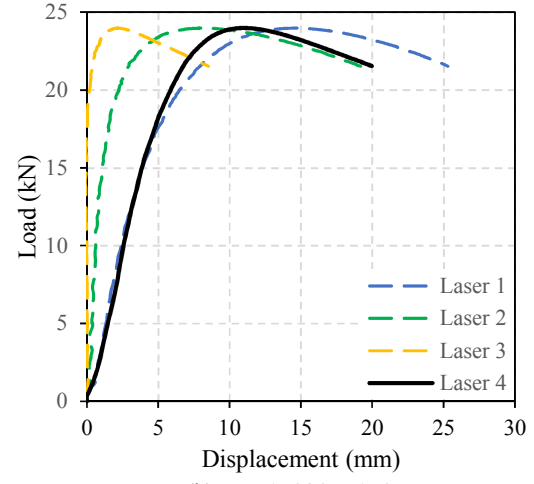
(b) Locations of web lasers



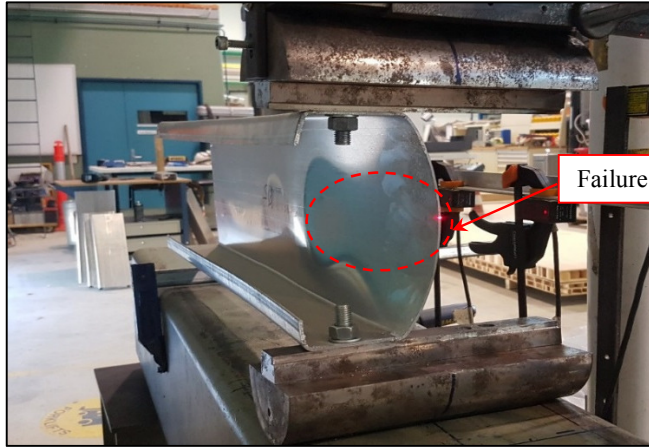
(c) Fastened ITF load case



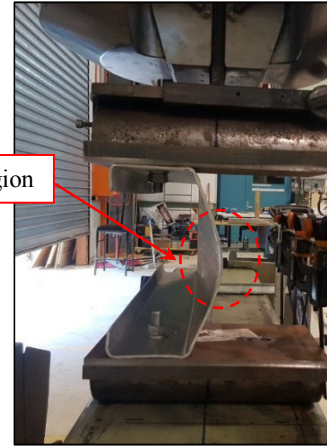
(a) ETF-20025-N150



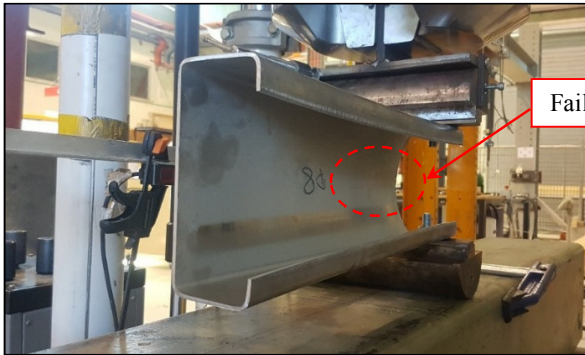
(b) ITF-15030-N150



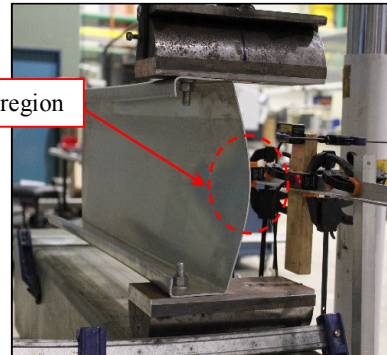
(a) ETF-20025-N25



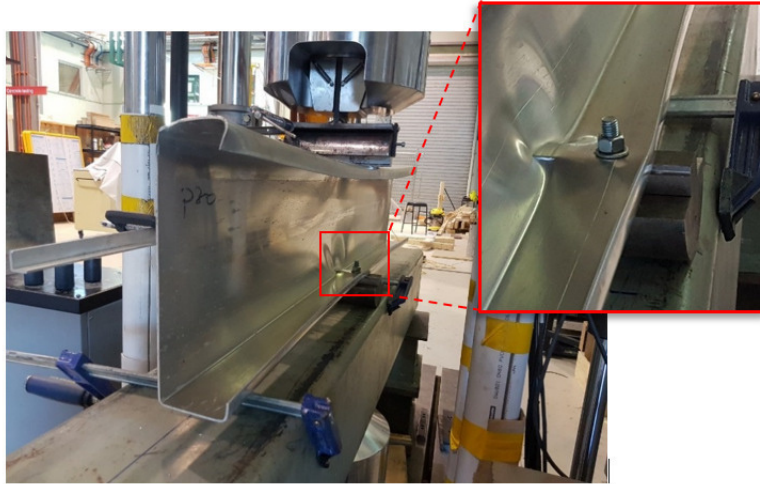
(b) ETF-20030-N150

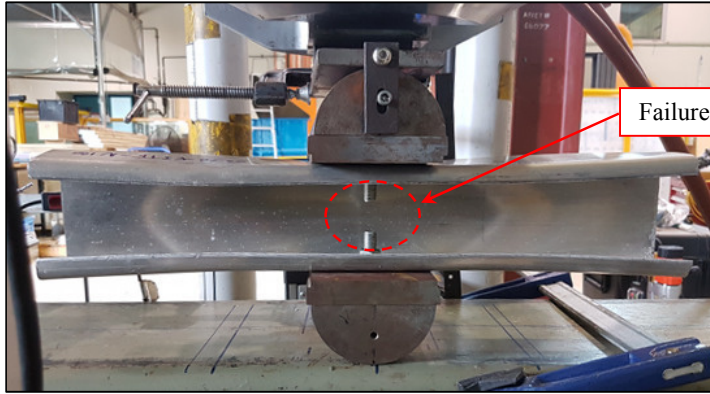


(c) ETF-15030-N25

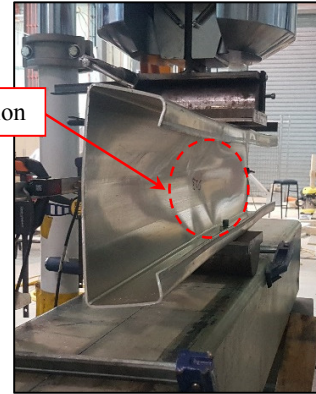


(d) ETF-25025-N100

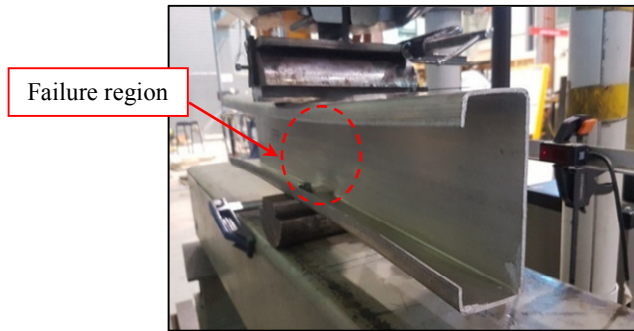




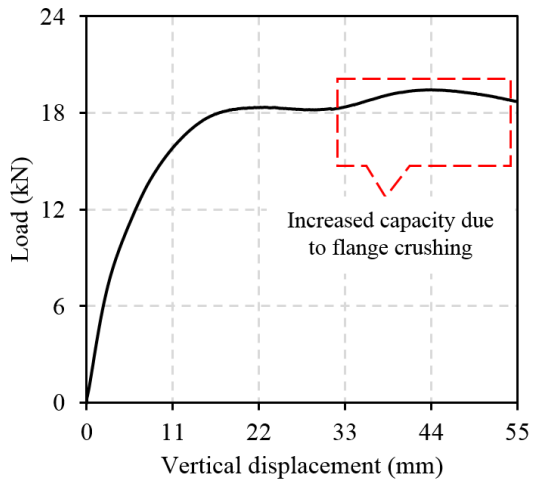
(a) ITF-10030-N100



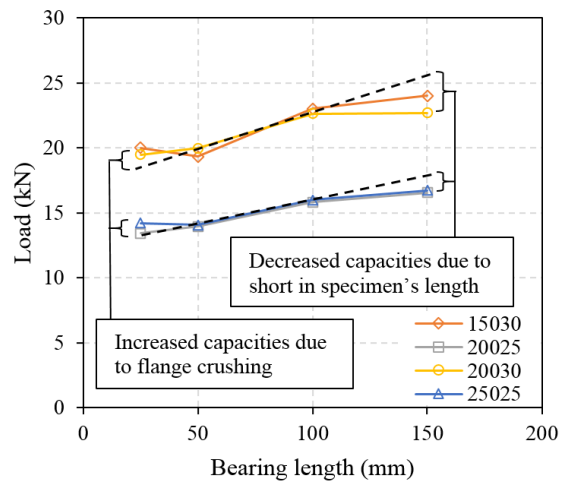
(b) ITF-20030-N150



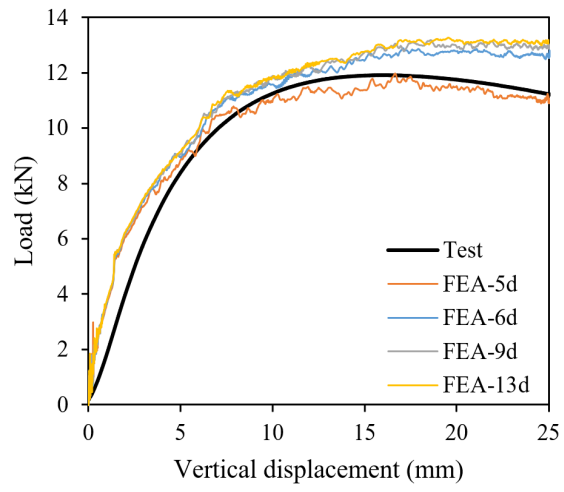
(c) ITF-15030-N50

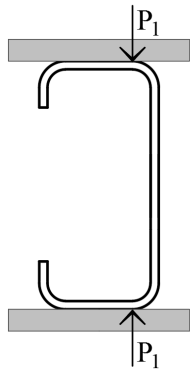


(a) Applied load versus vertical deflection (ITF-25025-N25)

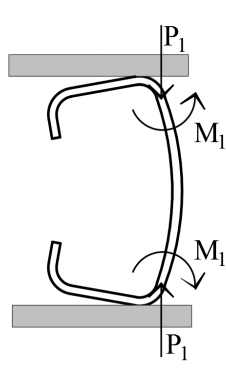


(b) Failure load versus bearing length – ITF load case

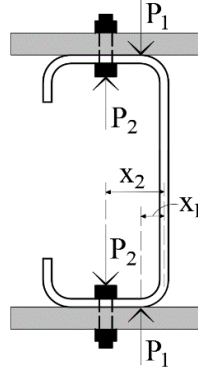




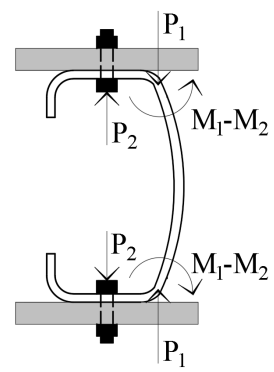
(a) Initial configuration (Unfastened)



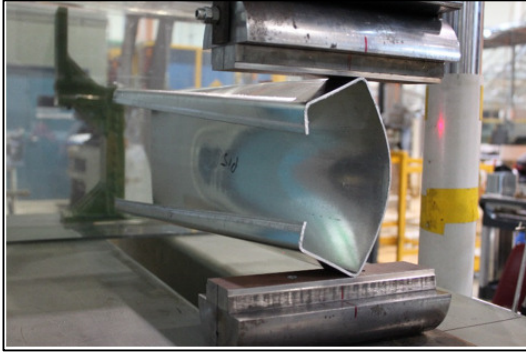
(b) Web and flange rotations (Unfastened)



(c) Initial configuration (Fastened)



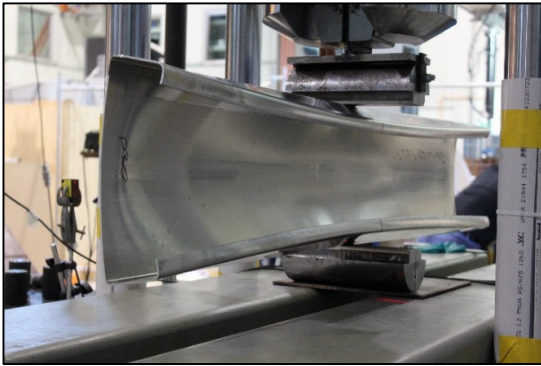
(d) Web rotation (Fastened)



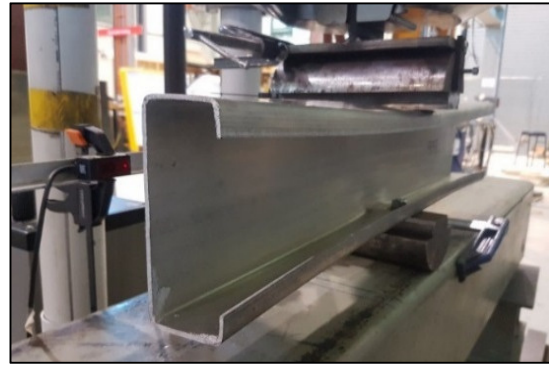
(a) ETF Unfastened



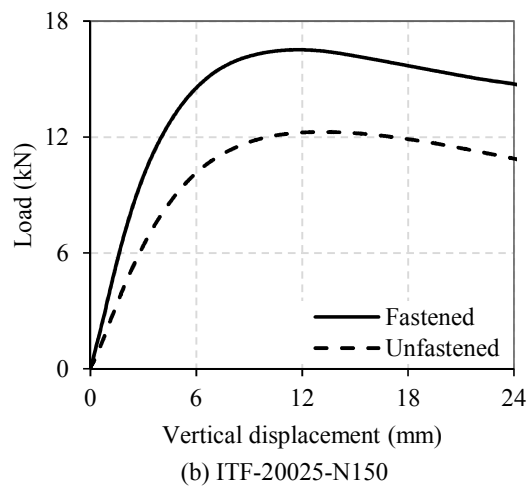
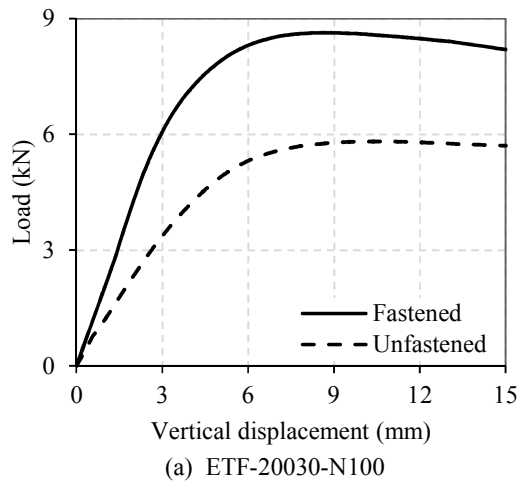
(b) ETF Fastened

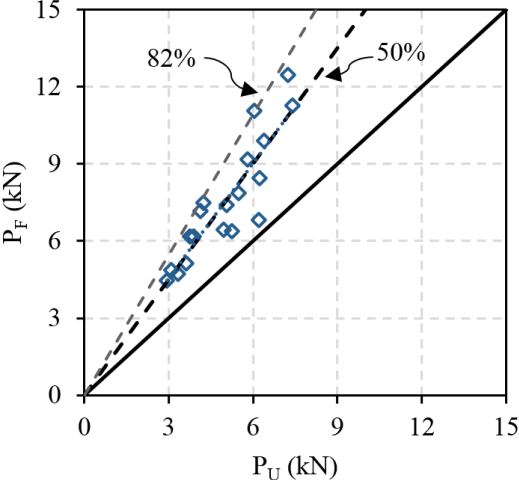


(c) ITF Unfastened

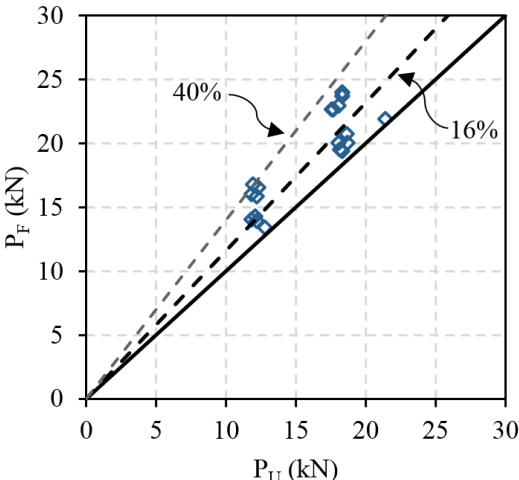


(d) ITF Fastened

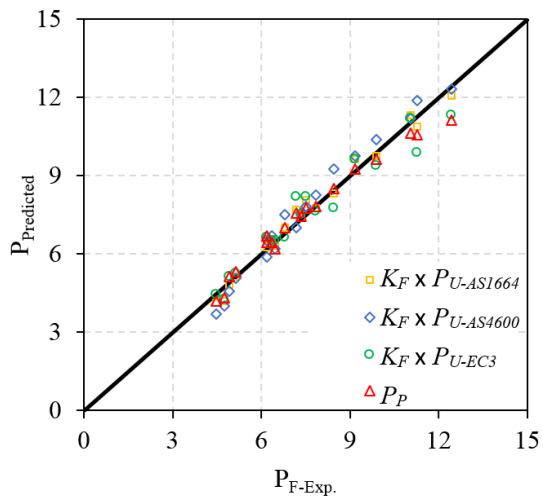




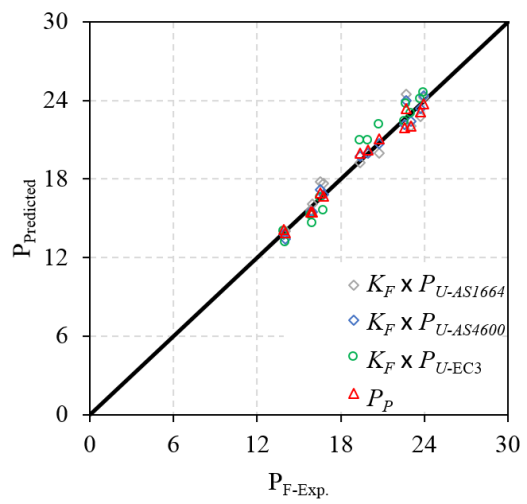
a) ETF load case



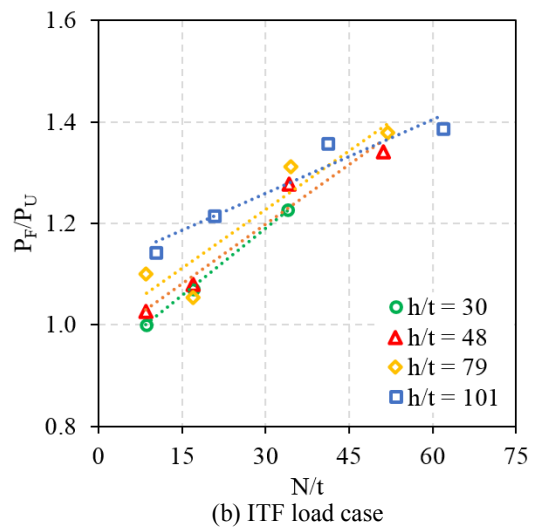
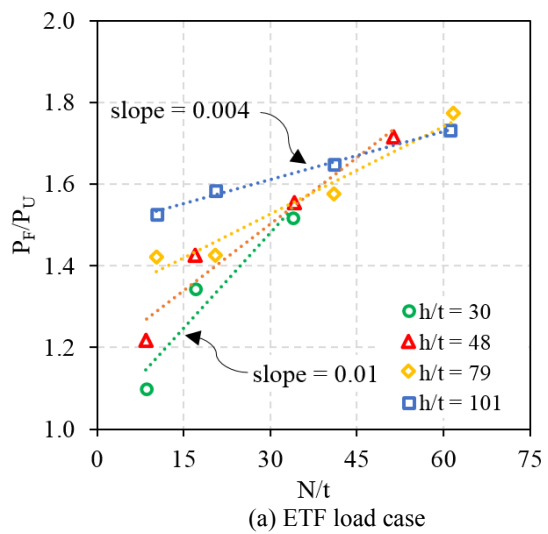
(b) ITF load case

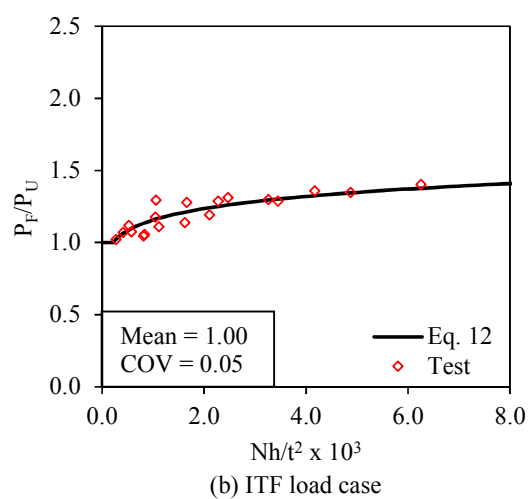
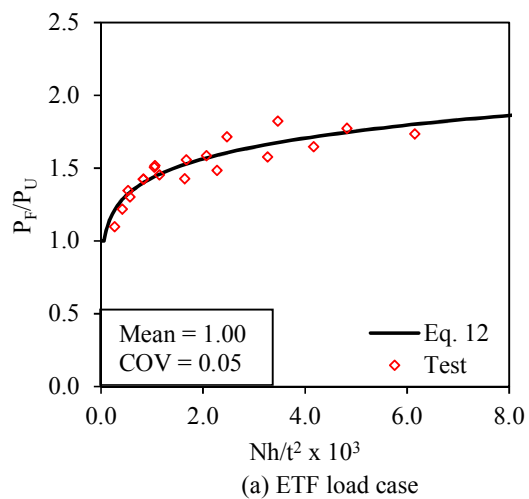


(a) ETF load case



(b) ITF Load case





- Fig. 1.** Application of roll-formed aluminium purlins, Minto reservoir – NSW, Australia
- Fig. 2.** Fastened two flange load case configuration
- Fig. 3.** Measured tensile stress-strain plot of structural aluminium alloy 5052 H36
- Fig. 4.** Web crippling test set-up
- Fig. 5.** Typical load versus deflection curves
- Fig. 6.** Web crippling failure modes under ETF load case
- Fig. 7.** Combined flange crushing and web crippling failure in ITF-25025-N25
- Fig. 8.** Web crippling failure modes under ITF load case
- Fig. 9.** Flange crushing failure mechanism
- Fig. 10.** Load versus vertical displacement curves for unfastened ITF-25025-N150 specimen with different lengths (Alsanat et al. (2019a))
- Fig. 11.** Unfastened and Fastened failure mechanisms for lipped channel cross-section subjected to a concentrated load
- Fig. 12.** Experimental web crippling failure modes for fastened and unfastened specimens
- Fig. 13.** Applied load versus vertical deflection responses for fastened and unfastened specimens
- Fig. 14.** Comparison between the experimental failure strengths of fastened (P_F) and unfastened data (P_U)
- Fig. 15.** Web crippling capacity predictions using the modified equations versus experimental web crippling capacities
- Fig. 16.** Web crippling capacity (P_F/P_U) ratios versus the bearing length to thickness ratios (N/t)
- Fig. 17.** Influence of fastened-to-unfastened capacity (P_F/P_U) against the geometrical factor Nh/t^2